北海道大学工学部研究報告
第175号（平成7年）

Bulletin of the Faculty of Engineering
Hokkaido University, No. 175 (1995)

Origin and Characteristics of Smilarity in the Structure of Turbulent Jet Diffusion Flames

Takemi CHIKAHISA and Tadashi MURAYAMA

(Received June 30, 1995)

Abstract

This paper describes similarities in temperature distribution and boundary layer characteristics in turbulent jet diffusion flames. Temperature distributions vary with the fuel, nozzle diameter, and jet velocity ; however, when temperature distributions are re-plotted in a non-dimensional manner using flame length, all data coalesces to a single curve, except for fuels with low volatility. Boundary layers of jets measured by Schlieren photographs were all straight and the angles were constant regardless of whether combustion was taking place or not.

The paper discusses the mechanism of the similarity, and shows a semi-theoretical flame length applicable for different fuels. Conservation of angular momentum in the vortex rings in the flame jet is the cause of the straight boundary. This mechanism leads to apparent reductions in air entrainment at the flame region, showing that the density change is the major cause of the phenomena ordinarily termed "laminarization".

As above, the phenomena are closely related to the turbulence structure, and laser tomography was applied to observe the eddy structure in the flames. The results showed apparent differences in the small scale eddies of non-flame and flame jets. It was also observed that air is entrained into the fuel by turbulent mixing, but combustion takes place by molecular diffusion in thin layers of fuel and air.

Introduction

In diffusion combustion, the combustion characteristics are functions of many complicated factors, and in diesel engines, for example, extensive work is still continuing to understand the structure of the flame and mixing process. Particularly in the engine field, there is no concept which enables correlation of combustion characteristics with injection speed, size of the nozzle, and fuel properties even for simple combustion system. Therefore the design of injection systems is based on trial and error development. Diesel spray combustion is not a steady state process, however a major part of the flame is considered similar to a steady jet flame [1-3]. To ensure optimum design of combustion systems and

Depeartment of Mechaninal Engineering, Hokkaido University Sapporo 060, Japan
Heat Energy Covesion Laboratory

a better understanding of combustion, it is essential to identify characteristics which enable a generalization of changes in combustion. One such characteristic observed in a variety of phenomena is similarity.

This paper shows similarities in the structure of turbulent jet diffusion flames, and discusses the mechanism of the similarity. To simulate a diesel spray flame, fuel is injected into stagnant air in the experiment. The results show a similar temperature distribution and boundary layer characteristics for various kinds of fuel, nozzle diameter and jet velocity. Theoretical considerations and observation of the microscopic eddy structure allowed a determination of a semi-theoretical flame length and the origins of the similarity.

There is much research on diffusion combustion, but most work is for furnace and burner combustion and little on the flames similar to diesel combustion. An important report of combustion characteristics which is helpful in the generalization is Onuma et al. who investigated similarity in the flame structure of spray and gas jet diffusion flames [4,5] . They compared droplet and temperature distributions, flow velocity, and gas composition in the flame of an air-atomizing burner. They showed that droplets within the flames do not burn individually with enveloping flames, but that a cloud of fuel vapor which they generate burns as a turbulent gas diffusion flame, and that the structure of the spray combustion flame is similar to that of the turbulent gas diffusion flame.

Theoretical research on turbulent jet flame length has been reported by, for example, Hawthorne et. al. [6], Chervinsky et.al.[7], and Peters [8]. They uses similarity assumption of boundary layer approximation or eddy viscosity in the jet, resulting in slightly different equations for the flame length. The results of the present research resemble the result of Peters somewhat, although the development of the equations are different. Peters also shows similarity in species and temperature when eddy viscosity (more precisely speaking, Chapman-Rubisin parameter) is assumed similar.

Experimental Apparatus

In the experiments here, gaseous and liquid fuels were injected vertically into stagnant air with nozzles of different sizes at speeds of 40 to 70m/sec and Reynolds numbers from 5×10^3 to 27×10^3. To hold the flame, a small pilot flame was set at the vicinity of the nozzle surrounding the jet. The flow speed was measured from the flow rate of the fuel and the nozzle area. The nozzles are simple hole nozzles to simulate the flame in, for example, diesel engines.

The temperature in the jet was measured by a 25 micron diameter Pt-Rd(13 %) thermocouple. To avoid errors in correction, the temperature was expressed by the measured value without correction for radiation.

Observation of the eddy structure of flames were performed with laser tomography in the manner reported by Shioji et. al. [9]. A 135mJ Nd-Yag laser was used as the light source. A 532 nm wave length 0.5 mm thick laser light sheet was used, and the Mie scattering of tracer particles was observed by a 35mm camera through an image intensifier

and optical filter. The tracer particles were titanium dioxide, T_iO_2, generated from titanium chloride, T_iCl_4, by reaction with water vapor in nitrogen gas. To remove the hydrochloric acid in the product, the reaction gas was bubbled through sodium hydroxide solution. The tracer in the nitrogen gas was introduced into the jet in the vicinity of the nozzle exit.

Experimental Results and Discussion

Similarity in Structure

Different temperature distributions in turbulent jet diffusion flames may be measured for various kind of fuel, nozzle diameter, and jet velocity. However, when the temperature distributions are re-plotted non-dimensionally as shown in Fig. 1, all the data arranges on one curve. In the figure, the axial temperature is non-dimensionalized by the theoretical adiabatic flame and ambient air temperatures, T_0 and T_∞ and the axial distance is normalized by flame length, x_r. The flame length was defined as the distance from the nozzle to the point of maximum temperature on the axis. The adiabatic flame temperatures were set at 2270K for LPG gas, 2190K for liquid [10], 2436K for methanol gas, 2331K for liquid, 2433K for normal-hexane, and 2566K for ethylene [11].

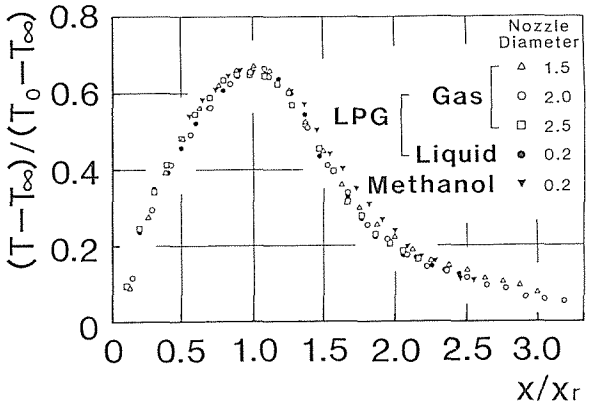

Fig. 1 Similarity in temperature distribution. The temperature is normalized by the adiabatic flame temperature and the axial distance is normalized by the flame length.

As Figure 1 shows, the temperature profiles of liquid and gaseous LPG flames as well as for different nozzle diameters were similar. Even methanol, with a stoichiometric air-fuel ratio of almost half of LPG, gives the same dimensionless temperature distribution as LPG. The actual flame became slightly longer as the velocity increased, but the dimensionless temperature profiles were identical for different velocities. Temperatures in the radial direction were also similar.

Figure 2 is Schlieren photographs of a non-flame N_2 jet and a methanol flame jet together with the flame picture. The figure shows the dimensionless distance normalized by

flame length. The boundary of the flame is straight and does not expand due to combustion. Additionally the angles of the jets are almost identical. A similar comparison was made with the LPG and hydrogen flames in reference [12], and also yielded an angle of about 14 degrees. This straight boundary layer is the major reason for the similar temperature profiles as will be discussed later.

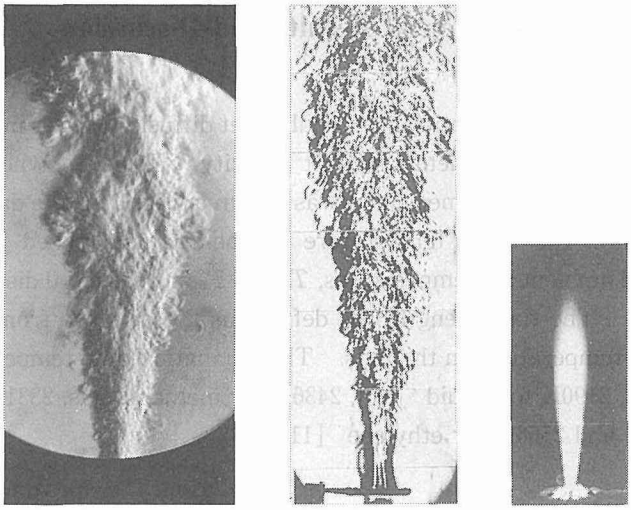

Fig. 2 Similarity in boundary layer configurations observed by Schlieren photography. Left is a non-flame N_2 jet and right a methanol flame, together with a picture of the flame.

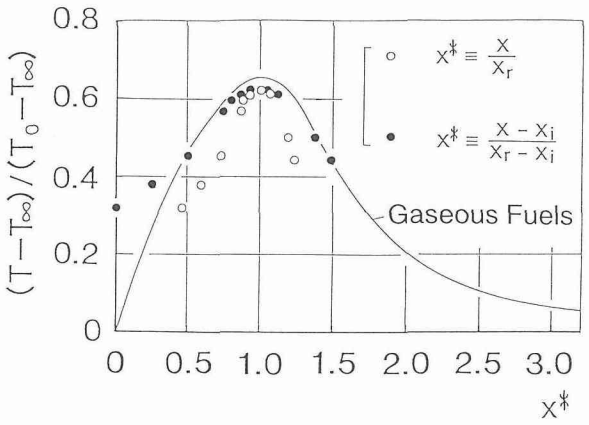

Fig. 3 Temperature profile in low volatile fuel (normal-hexane). The sift in the virtual origin of the jet coordinates maintains similarity.

Generally, fuels which are less volatile than methanol show thinner, longer flames, and the temperature distribution does not arrange on the above mentioned similarity curve.

Figure 3 is the results with normal-hexane. The open circles are very different from the curve for the gaseous fuels. However, if the distance from the nozzle is modified to an imaginary downstream nozzle position, as a virtual origin of the jet, the axial temperatures become similar like the solid circles. Thus the volatility of the fuel affects the point of origin of the similarity but does not affect similarity itself, except for very low volatile fuels.

Theoretical Flame Length and Temperature Distribution

If the straight boundary is accepted as a starting point for the discussion, it is possible to derive a semi-theoretical flame length and air entrainment for a variety of nozzle conditions and fuels.

Similar to Ref. [13], the following dimensionless parameters are defined:

$$u^* \equiv u/u_0, \quad x^* \equiv x/d_0$$

$$\rho^* \equiv \rho/\rho_0, \quad I^* \equiv (I-I_\infty)/(I_0-I_\infty) \qquad \text{Eq. (1)}$$

$$\delta^* \equiv \frac{(Y_fL-Y_a)-(Y_fL-Y_a)_\infty}{(Y_fL-Y_a)_0-(Y_fL-Y_a)_\infty} = \frac{Y_fL-Y_a+1}{L+1}$$

The δ^* is the dimensionless species mass fraction corresponding to the fuel fraction in a non-flame jet.

Then the conservation equations and boundary conditions of momentum, energy, and species can be expressed in exactly the same forms by extending Ref. [13] for variable density, when equal transport of heat, mass, and momentum is assumed, e.i. turbulent Lewis and Prandtl numbers equal unity. As a result the solutions to these equations, e.i. axial velocity, enthalpy, and species, must be identical in dimensionless form as;

$$u^* = I^* = \delta^* \qquad \text{Eq. (2)}$$

The momentum equation and subsequent axial velocity become as follows:

$$M = \int 2\pi\rho u^2 r dr = 2\pi b^2 \rho_m u_m^2 f(\eta)$$

$$= \rho_0 u_0^2 \pi d_0^2/4 \qquad \text{Eq. (3)}$$

$$\therefore \quad u_m^* = A(\rho_0/\rho_m)^{1/2} d_0/x$$

where the density and the axial velocity are assumed to be a function of η when they are normalized by the values on the axis, and the η function is assumed to be constant at any x section.

Assuming perfect diffusion control combustion, fuel and air fractions, Y_f and Y_a, are zero at the flame. Substituting this into the δ^* in Eq. (1), and from Eqs. (2) and (3), one obtains the flame length as follows:

$$x_r = A(L+1)(\rho_0/\rho_r)^{1/2} d_0 \qquad \textit{Eq. (4)}$$

This flame length is applicable for a variety of fuels and nozzle injection conditions.

Similar to the derivation in Ref. [13], one can obtain analytical temperature distribution. Enthalpy is expressed as a function of temperature as follows:

$$I=\sum_i (Y_i c_{pi})\, T + Y_f H_u = I^*(I_0 - I_\infty) \qquad \text{Eq. (5)}$$

For simplicity, it is assumed that the specific heats of fuel, air, and product are identical. At the flame, the assumption of perfect mixing control combustion gives $Y_f = Y_a = 0$, so that Eqs. (1) and (5) become

$$\begin{aligned} \delta_r^* &= 1/(L+1) \\ T_r - T_\infty &= I_r^* H_u / c_p \end{aligned} \qquad \text{Eq. (6)}$$

because $(I_0 - I_\infty) = H_u$ and $I_\infty = c_p T_\infty$.

Substituting Eq. (2) into Eq. (6) and from Eq. (5), the following analytical temperature distribution is obtained:

$$\begin{aligned} T^* &= (L+1)(1-u^*)/L \quad (\textit{inside of flame}) \\ T^* &= (L+1)\, u^* \quad (\textit{outside of flame}) \end{aligned} \qquad \text{Eq. (6)}$$

where T* is the dimensionless temperature defined by the adiabatic flame temperature and the ambient temperature as in Fig. 1.

Discussion of the Theoretical Flame Length and Air Entrainment

Defining $X^* \equiv x/x_r$, Substitution of Eqs. (3) and (4) into Eq. (7) shows that downstream of the flame the dimensionless temperature is a function of only X^*, and upstream of the flame it is a function of X^* and the stoichiometric air-fuel ratio. This indicates that when the straight boundary is established the similar temperature distribution can be explained theoretically based on momentum, energy, and species conservation.

Table 1 compares measured constant A values in Eq. (4) for a variety of fuels and

Table 1. Measured flame lengths and the corresponding constant A values in the flame length equation.

Fuel	Non Flame jet	LPG	-	-	-	CH_3OH	-	C_2H_4	-	-
Phase	Gas	Gas	-	-	Liq.	Gas	Liq.	Gas	-	-
L		15.6	-	-	-	6.47	-	14.7	-	-
d_0		1.5	2.0	2.5	0.2	2.0	0.2	1.5	2.0	2.5
Xr		360	400	510	510	185	551	280	285	330
$(\rho_f/\rho_r)^{1/2}$	1	3.01	3.01	3.04	47.4	2.19	60.8	2.17	2.24	2.23
$(\rho_f/\rho_{r0})^{1/2}$		3.55	3.55	3.55	58.8	2.69	72.0	2.88	2.88	2.88
A: $[\rho_r]^{a)}$	5.00	4.80	4.00	4.04	3.24	5.65	6.07	5.48	4.05	3.77
A: $[\rho_{r0}]^{b)}$		4.07	3.39	3.46	2.61	4.60	5.12	4.13	3.15	2.92

a) The constant A was derived from measured ρ_r. b) Derived from ρ_{ro}.

nozzle conditions. In the table ρ_{r0} and ρ_r are densities at the flame calculated from the adiabatic and measured flame temperatures. The results show that the constant value of A calculated from the measured flame density is approximately 5.0 even for very different fuel densities and stoichiometric air-fuel ratios: for example the density of gas is less than 1/20 that of liquids, and the stoichiometric air-fuel ratio of LPG is half that of methanol. Here, the constant value calculated from the measured flame density is the same as in a non- flame jet. The results indicate the validity of Eq. (4).

When the density calculated from the adiabatic flame temperatures are used, the constant value becomes approximately 4.0. As adiabatic flame temperatures are calculated, they may be easier to apply than using the actual flame temperatures. Among the constants, the liquid LPG shows a smaller A value than the others. This may be attributed to the fact that the fuel evaporates very rapidly and as the actual fuel density at the nozzle is somewhat less than the pure liquid density.

The axial temperature change, T_m^*, can be solved analytically by considering the density change due to combustion. As density is inversely proportional to temperature in a constant pressure field, substitution of Eqs. (3) and (4) into Eq. (7) leads to a temperature change along the axis, downstream of the flame as follows:

$$T_m^* \propto 1/X^{*2} \qquad \textit{Eq.}\ (8)$$

where approximation was made with $T_w/T_r \approx T_m^*$.

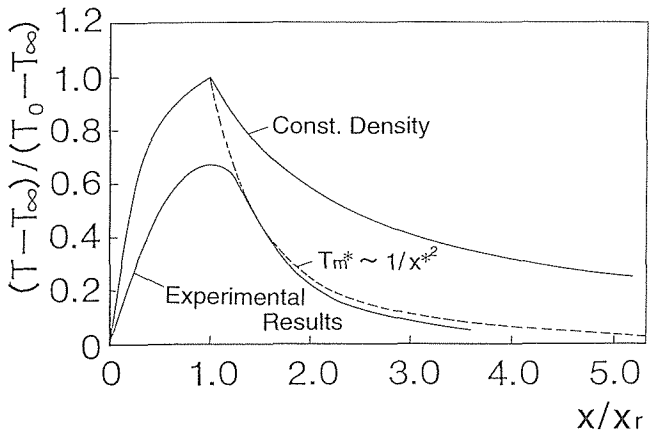

Fig. 4. Comparison of analytical temperatures and experimental results. The curve of $T_m^* \sim 1/x^*$ takes density changes due to combustion into account.

Figure 4 shows the analytical temperature curves and experimental results, in which ρ=constant corresponds to the imaginary case where combustion takes place at the same mixing rate as in the non-flame case; this imaginary condition gives $T^* \propto 1/x^*$ downstream of the flow. The variable-density line fits well with the experimental results, validating the above analysis.

The quick temperature decrease in the variable-density case indicates that air entrainment increases as the temperature decreases in the flow direction, in other words, air entrainment decreases in the flame region. Here it must be noted that flame lengths of variable-density jets is longer than in the constant-density case, and the abscissa is non-dimensionalized by these flame lengths. Thus the figure does not mean that the variable density case has larger air entrainment, but indicates that the air entrainment is decreasing at the flame region. A comparison of the two analytical curves indicates that the reduction in air entrainment in the flame region is mainly due to density changes. The disappearance of small eddies in the flame (shown below in Fig. 6) does not affect the entrainment significantly, as the analysis does not take the difference in small eddies into account.

Mechanism of the Similarity

The previous discussion is based on straight boundary considerations, and this section discusses the mechanism working to maintain the straight boundaries. Assuming that vortex rings are emitted continuously from the nozzle, the air entrainment is considered proportional to the number-density and intensity of vortex rings in a unit area, as air is entrained into the jet by turbulent vortices. Angular momentum of the vortex rings may be considered to be conserved in a similar manner as in momentum conservation of jets, although the momentums actually dissipate in both cases. The continuity equation of angular momentum of the vortex rings is as follows:

$$\rho\Gamma_e n V_e = (\rho\Gamma_e n V_e)_0 \propto \rho_0 u_0^2 d_n^3 \qquad \text{Eq. (9)}$$

An equation of number-density of vortex rings in a section parallel to the axis is

$$n/\left(\int_0^{b/2} u dr\right) = n/\left\{u_m b \int_0^{\eta} u^*(\eta)\, d\eta\right\} \propto n/(u_m b) \qquad \text{Eq. (10)}$$

where the integral of $u^*(\eta)$ is assumed constant at any x position, as above.

The product of the angular momentum of one vortex ring and the number-density of the vortices, i.e. product of Eqs. (9) and (10) divided by n, is assumed proportional to the air entrainment rate in a unit axial length, and will be termed the angular momentum density of vortices in the following. However the dimension of the angular momentum density of vortices is different from that of the air entrainment rate. Jets from different nozzle diameters have the same air entrainment rate if Reynolds numbers are identical, while the angular momentum density of vortices increases with nozzle diameter. This indicates that the air entrainment rate is proportional to the angular momentum density of the vortices divided by nozzle diameter. Thus the air entrainment rate becomes

$$\dot{m}_x \propto (\rho\Gamma_e n V_e)_0/(u_m b d_n) \propto (\rho_0 u_0^2 d_n^2)/(u_m b) \qquad \text{Eq. (11)}$$

where $\dot{m}_x$ is the air entrainment rate from the surrounding in a unit axial length.

Then the continuity equation is

$$\dot{m}_x = \frac{d}{dx}\int_0^{b/2} 2\pi\rho u r dr \propto \frac{d}{dx^*}\rho_m^* u_m^* b^{*2} \qquad \text{Eq. (12)}$$

Similar to Ref. [14], with $b \propto x^p$, $u_m \propto x^q$, and $\rho_m \propto x^s$, dimension analysis shows the shape of the boundary for the equations of momentum and continuity ; Eqs. (3) and (2). The result showed that the only solution is $p = 1$, indicating straight boundary even for non-uniform gas densities along the axis.

A physical interpretation of the analysis shows that the boundary may expand after ignition, but that the air entrainment decreases inversely proportional to b and u_m in Eq.(11) until the boundary becomes straight. The decrease in air entrainment is caused by a decreased number-density of vortex rings due to expansion. As shown in Fig. 5, the jet expands at ignition and at extinguishment but in the steady state the boundary is maintained straight.

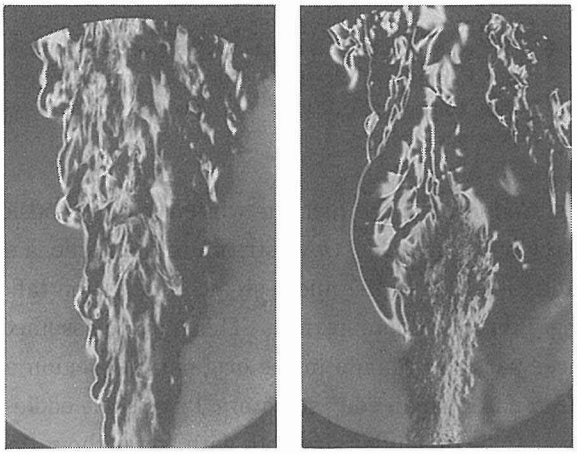

Fig. 5. Schlieren photographs of steady jet flame (left) and flames at the moment when the pilot flame is extinguished (right). A straight boundary is maintained only at the steady state condition.

In the above discussion, the equation which correlates air entrainment rate and vorticity is not entirely satisfactory because of the mismatch of dimension. Additionally the direct force on the air entrainment is a pressure difference rather than the turbulence itself, and the pressure difference is caused by the turbulent diffusion. Thus further investigation is necessary to establish the mechanism of the similarity.

Micro-Structure of Eddies

To understand the turbulence in the jet flames, the microscopic eddy structure was observed with laser tomography. Figure 6 shows such an image of the situation with and without flame. It is clear that tracer particles diffuse more in the non-flame jet, and that there is an apparent eddy structure in the flame jet. This indicates that micro-scale eddies decay in the flame due to higher molecular viscosity.

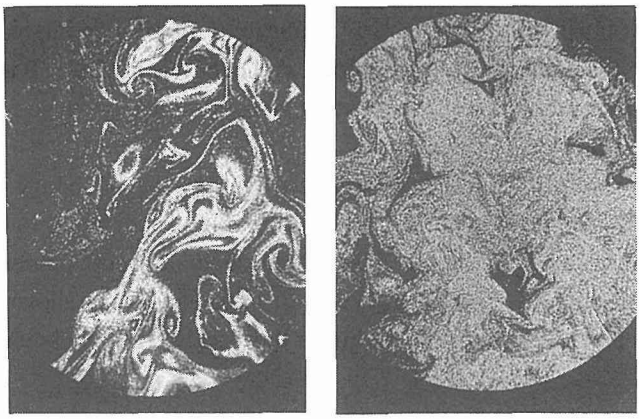

Fig. 6. Micro-structure in a ethylene flame jet (left) and in a non-flame jet of N_2 (right). The pictures are taken by laser tomography at $x/d_0=300$, and the size of the view is about 60mm.

As tracer particles are mixed in the fuel, the white region is considered to be a fuel rich region while the dark region is air rich. Downstream of the flame, a similar striped pattern was also observed, indicating that at the micro-sscale combustion takes place by molecular diffusion even in strongly turbulent combustion. This may be assumed as the tracer follows the bulk flow and tracer particles remain in the original fuel region after combustion.

Even with this difference in small eddy structure, large scale eddies, which correspond to the integral scale, appear to be of similar size both with and without flames. This result and the analysis in the previous section suggests that air entrainment is closely related to large scale eddies and independent of small scale eddies, while the micro structure in the eddies may affect the emission formations if emissions are formed in the thin layers of fuel and air.

Conclusions

Characteristics of turbulent jet diffusion flames were observed for a variety of fuels and injection conditions, and theoretical considerations were used to elucidate the mechanism of the similar structures. The conclusions of the investigation are as follows:

1. Similar temperature distributions and identical boundary configurations were found for various kinds of fuel, nozzle diameter, and jet velocity, when fuel is injected from a simple hole nozzle. The angle of the straight boundaries was constant both with and without flame.
2. Theoretical considerations explained the mechanism of the similar temperature distribution, and it also derived the flame length which is applicable for different fuels.
3. The mechanism of the straight boundary was partially explained theoretically, based upon angular momentum conservation of vortices. However further theoretical development is necessary for a full explanation.

4. The micro structure in the turbulent mixing process was shown with laser tomography: air is entrained into jets by large scale eddies and combustion takes place by molecular diffusion between striped pattern micro layers of fuel and air.

Acknowledgement

The authors wish to express their appreciation to Dr. M. Konno and Mr. K. Kikuta, research associates of Hokkaido University (Dr. Konno is now an assistant proffessor at Ibaraki Uuiversity), and the following graduate students for their contribution to the experiments: Mr. K. Takenawa, T. Sugesawa, T. Masuda, M. Kodo, K. Umeda, T. Matsumoto, S. Joco, H. Ashie, and T. Araki.

Nomenclature

A : constant
b : width of boundary layer, m
c_{pi} : specific heat of species i, kJ/kg•K
d_0 : nozzle diameter, m
H_u : lower heating value of fuel, kJ/kg
I : enthalpy, kJ/kg
L : stoichiometric air fuel ratio
$\dot{m}_x$: air entrainment rate, kg/m•s
M : momentum, kg•m/s^2
n : production rate of vortex ring numbers, 1/s
r : radius, m
T : temperature, K
T_0 : adiabatic flame temperature, K
u : velocity, m/s
u_0 : injection velocity, m/s
V_e : volume of a vortex ring, m^3
x : axial distance, m
x_r : flame length, m
X^* : dimensionless length; x/x_r
Y_i : mass fraction of species i
δ : normalized species fraction
Γ : circulation, m^2/s
η : dimensionless radius; r/b
ρ : density, kg/m^3
ρ_{r0} : density at adiabatic flame temperature, kg/m^3

Subscript

a : air

e : eddy (vortex ring)

f : fuel

m : center axis

r : flame

0 : nozzle exit condition

∞ : ambient condition

Superscript

* : dimensionless quantity

References

1) Wakuri, Y., Fujii, M., Amitani, T., and Tsuneya, R., Bulletin of the Japan. Soc. Mech. Eng. 13-3 : 123 (1960)
2) Nakagawa, H., Tateishi, M., and Sekino, M., Trans. SAE 760214 (1976), 1002-1018
3) Chikahisa,T., and Murayama, T., 20th International Congress on Combustion Engines, CIMAC, London, D47 (1993), 1-20
4) Onuma, Y., and Ogasawara, M., 15th Syimposium (international) on Combustion, The Combustion Institute, Tokyo, (1974), pp 453-465
5) Onuma, Y., Ogasawara, M., and Inoue, T., 16th Symposium (International) on Combustion, The Combustion Institute, Cambridge, (1976), pp 561-567
6) Hawthorne, W.R., Weddell, D.S., and Hottel, H.C., 3rd Symposium on Combustion, Flame and Explosion Phenomena, The Combustion Institute, Madison, (1949), pp266-288
7) Chervinsky, A., and Manheimer-Timnat, Y., Combust. Flame 13 : 157-165 (1969)
8) Peters, N., lnternational Chemical Engineering 25-3 : 406-417 (1985)
9) Shioji, M., Yamane, K., Isogami, H., and lkegami, M., Trans. of Japan Soc. Mech. Eng., B-57-542 : 3562-3568 (1991)
10) Mizutani, Y., Combustion Engineering, Morikita Publishing, Tokyo, 1984, p66
11) JSME Mechanical Engineers' Handbook, Japan Society of Mechanical Engieers, Tokyo, 1985, p 73
12) Chigier,, N ., Energy, Combustion, and Environment, McGraw-Hill, New York, 1981, p 215, p 232
13) Ablamovich, G., The Theory of Turburent Jets, MIT Press, New York, 1963, pp345-363
14) Rajaratnam, N., Turbulent Jets, Elservier Scientific Publishing, Amsterdam, 1976, p 7